



ELSEVIER

Available online at www.sciencedirect.com

SCIENCE @ DIRECT®

annals of
NUCLEAR ENERGY

Annals of Nuclear Energy 31 (2004) 1415–1428

www.elsevier.com/locate/anucene

Technical note

Image reconstruction techniques using projection data from transmission method

A.M. Ali ^{a,*}, Z. Melegy ^d, M. Morsy ^d, R.M. Megahid ^a,
T. Bucherl ^b, E.H. Lehmann ^c

^a *Reactor and Neutron Physics Department, Nuclear Research Center, Atomic Energy Authority, P.O. Box 13759, Cairo, Egypt*

^b *Institut Für Radiochemie, TUM, Munchen, Germany*

^c *Paul Scherrer Institute, Villigen, Zurich, Switzerland*

^d *Faculty of Science, Ain Shams University, Cairo, Egypt*

Received 6 October 2003; accepted 12 March 2004

Available online 10 May 2004

Abstract

This paper gives a brief description of a filter back projection (FBP) and Algebraic Reconstruction techniques (ART), which are used for reconstruction of projected data obtained from transmission measurements. Both techniques are tested by reconstructing a simulated object, showing that the FBP technique yields images with better resolution and higher contrast, thus resulting in more accurate information than obtained by ART.

Experimental data has been obtained for unheated and heated ordinary and heavy concrete samples by transmission measurements using a thermal neutron beam emitted from the spallation neutron source SINQ at PSI, Switzerland. The data are used to reconstruct the images of the examined samples using the FBP technique with different filter functions, including the Shepp Logan filter function produces images of higher contrast, more smoothing and slightly better resolution than those obtained using the absolute filter function. Based on these images the samples were investigated for water content, cracks, homogeneity, etc.

© 2004 Elsevier Ltd. All rights reserved.

1. Introduction

The method of computerized tomography (CT) for providing three dimensional information about the internal structure and the elemental distribution within the

* Corresponding author.

investigated object has proven itself as a versatile technique for non-destructive testing of materials of prime importance in nuclear and general industries (Schatz et al., 1989). Neutrons are attenuated by interactions with the nuclei of the atoms contrary to photons, which interact mainly with the shell electrons. Accordingly, the neutron CT-images will show different information compared with X-ray or gamma-ray tomography, where neutron imaging gives information on nearby elements in the periodic table and different isotopes of the same element due to the irregular values of neutron attenuation coefficient.

For most elements, neutrons with energy $E > 0.1$ MeV will have cross section smaller than thermal neutrons, especially for heavy atoms. Therefore, fast neutrons are very useful for examining large metallic objects. The fast neutron cross section of hydrogen is about 1 b, approximately one order of magnitude larger than the corresponding X-ray cross section. Compound materials containing metals and plastics are ideal objects for fast neutron tomography, and small differences in hydrogen concentrations can be detected. Also, in the energy range from about 1 eV to 0.5 MeV, many atoms show sharp resonance in the cross sections. Therefore with appropriately filtered neutron beams, a selective search for special materials is possible. For example silicon has an anomalous by large cross section at 143 keV and could lead to some CT-research applications in geology and petrology.

However thermal neutrons are used to investigate ceramic materials, the detection of corrosion products and to examine the water content of some materials. Also, thermal neutron tomography may be used to examine small samples containing hydrogen-like aluminum and its corrosion products (Pfister et al., 1992; Ali, 1998).

2. Basic concepts

The image reconstruction techniques use the measured projection data as input to calculate the density distribution of the desired cross section of the investigated sample as output. Accordingly, the two dimensional image of the desired cross section can be obtained. The applicable reconstruction techniques are divided into three categories, first back-projection reconstruction, second by iterative reconstruction, and third by analytical reconstruction. Filtered Back Projection (FBP) technique will be introduced as an example of the back-projection reconstruction technique; however, the Algebraic Reconstruction Technique (ART) technique will be introduced as an example of an iterative reconstruction technique. A brief discussion of the FBP and ART is given below.

2.1. Filtered back projection technique

The FBP image reconstruction technique is used in most commercial medical scanners and has proved to be extremely accurate and amenable to fast implementation. This technique can be given a rather straightforward intuitive rationale because each projection represents a nearly independent measurement of the object.

This is not obvious in the space domain but if the Fourier transform is found of the projection at each angle then it follows easily by the Fourier Slice Theorem (Avinash and Malcolm, 1999). The projections are nearly independent because the only common information in the Fourier transform of the two projections at different angles is the dc term, which has been constructed at zero frequency, thus the Fourier transformer expresses the average of all projections i.e

$$F(0) = \frac{1}{N} \int_{-\infty}^{+\infty} P_{\theta}(t) dt, \quad (1)$$

where $F(0)$ is the Fourier transform of projection data at zero frequency, $P_{\theta}(t)$ is the projection data at certain angle θ , N is the number of transmission and t is the transmission value.

The FBP algorithm can be summarized as follows;

First, the measured projection data at different angles (equiangular steps) have to be obtained; the Fourier transform of the projection data has to be estimated by the following Fourier form;

$$F(\omega) = \frac{1}{N} \int_{-\infty}^{+\infty} P_{\theta}(t) \exp \left\{ -i \frac{2\pi}{N} \omega t \right\} dt, \quad (2)$$

where $F(\omega)$ is the Fourier transform of projection data at frequency ω .

This Fourier transform data will be filtered with the absolute function $|\omega|$ or with the Shepp Logan function (Shepp and Logan, 1974) $|\omega| * (\sin(\omega)/\omega)$, and the obtained data will be back projected to have the distribution of the linear attenuation coefficients.

The Fourier transform method is fast and easy to be implemented, but for optimum performance, equiangular projections over 180° are needed. This method was applied in the computer code for neutron CT image reconstruction and various filter functions can be used depending on the structures to be visualized in the CT-image (Avinash and Malcolm, 1999).

2.2. Algebraic reconstruction technique

An entirely different approach for tomographic imaging consists of assuming that the cross section consists of an array of unknowns and the setting up algebraic equations for the unknowns in terms of the measured projection data. Although conceptually this approach is much simpler than the transform-based methods, for medical applications at least 1% density resolution is required which cannot be obtained by ART technique, thus it lacks the accuracy in density resolution and the speed of implementation. However, there are situations where it is not possible to measure a large number of projections, or the projections are not uniformly distributed over 180° , both these conditions are being necessary for the transform-based techniques to produce results with an accuracy acceptable for medical imaging.

All algebraic reconstruction technique methods are iterative procedures. That is, first starting with an initial guess for the image function $\mu(i, j)$ for each pixel (i, j) of the reconstructed image,

$$\mu(i, j) = \text{constant}; \quad i = 1, \dots, N \quad j = 1, \dots, N. \quad (3)$$

The projection data through the reconstructed image are calculated for a certain angle θ , using the relation;

$$P_{\text{calculated}}(\theta) = \int_L \mu(i, j) dl; \quad L \text{ path of the incident ray.} \quad (4)$$

Comparison between the calculated and measured projection data has been made, and the difference between them is calculated by

$$\Delta P(\theta) = P_{\text{calculated}}(\theta) - P_{\text{measured}}(\theta) \quad (5)$$

The image function for each pixel will be modified depending on the difference Δp between the calculated and measured projection,

$$\mu_k = \mu_{k-1} + \left(a_i * \Delta p_i / \sum a_i^2 \right), \quad (6)$$

where k is the number of iteration, a_i is the area of i th pixel and $\sum a_i^2$ is the summation of square area of all pixels within the ray.

Eqs. (3)–(5) are repeated until the difference between the calculated and measured projections can be neglect.

3. Experimental details

3.1. Experimental arrangement

Small samples of diameter 5 cm of ordinary and heavy concretes are scanned at the thermal neutron radiography station NEUTRA at the Paul Scherrer Institute, Switzerland. As illustrated in Fig. 1, the radiography station consists of three main components: the inner collimator which is fixed inside the target block shielding (including the main shutter), the outer collimator which is an evacuated divergent aluminum tube and the working room which is shielded with concrete blocks. The radiography station NEUTRA uses one of the four twin-beam lines for thermal neutrons at SINQ. The thermal neutron spectrum is mainly determined by the moderator (heavy water), the position where the beam tube nozzle looks into the moderator tank and the bismuth crystal placed in the beam line for gamma background reduction. The NEUTRA is 13.131 m apart from the target center, so it is suitable for routine use because of its high collimation ratio, large beam diameter and the amount of free space for sample handling. The outer collimator is of 40 cm, diameter, but the active diameter is of 25 cm, which associated with nearly constant flux.

Fig. 2 shows the NEUTRA at SINQ facility at that interim position which consists of these three main components:

- The shielding support with a vertical channel for guiding downward and upward movement of the samples.

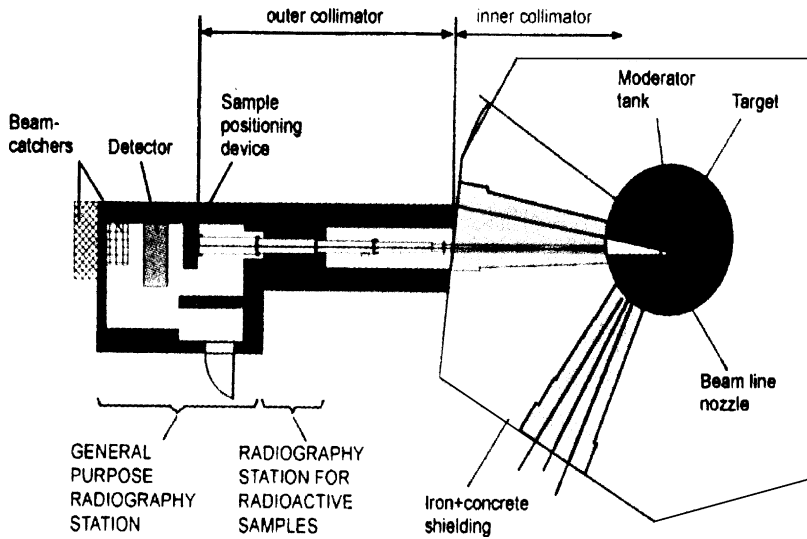


Fig. 1. General layout of the NEUTRA facility at a thermal beam line of the spallation neutron source SINQ.

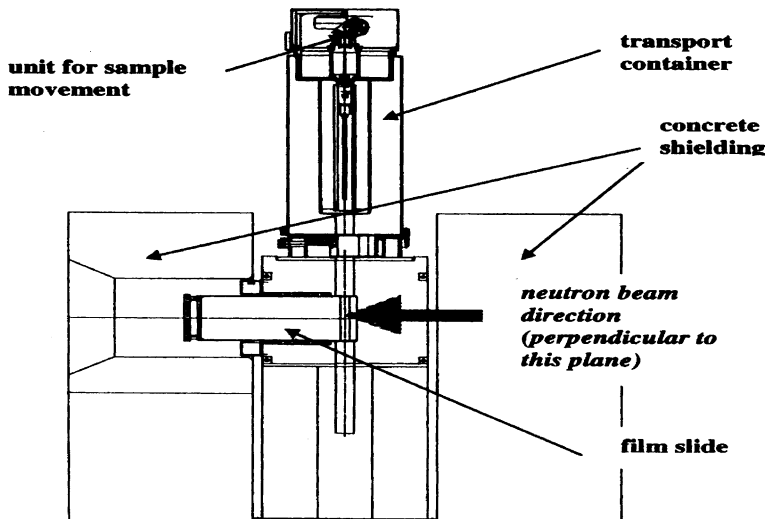


Fig. 2. Radiography station NEUTRA in use for investigations of highly activated samples.

- The upper steel shielding block with a penetration for the neutron beam, and space room for the sample and the detector holder.
- The transport cask which is made of lead shielding of about 20 cm thickness and stainless steel walls. This cask is also used for the remote positioning of the samples in the beam and for height and angular movements (Lehmann et al., 2001).

3.2. Detection system

The detector is one of the main components for the setup for experimental neutron radiography. The thermal neutrons that pass through the sample are recorded by a CCD-camera system. The basic principle of the detector is the combination of the CCD-camera with a neutron-sensitive scintillator screen (see Fig. 3). The light from the screen is reflected to the camera by a mirror and focused on the CCD-chip by a special lens. The CCD-camera has the highest dynamic range, very good linearity and reproducibility, but its spatial resolution is limited. Using a video and fast CCD-cameras it is possible to achieve the best dynamic resolution for real-time imaging but the dynamic range is limited (Pleinert et al., 1997).

3.3. Concrete samples under investigation

Unheated and heated samples of ordinary concrete ($\rho = 2.3 \text{ gm/cm}^3$) and heavy hematite concrete ($\rho = 2.9 \text{ gm/cm}^3$) of 5 cm, diameter have been investigated. The samples have been prepared at the Institute fur Radiochemie, TU Munchen. Both ordinary and heavy concretes are scanned and then heated at 110 °C for 7.5 h and then heated at 200 °C for 15 h.

3.4. Scanning procedure

The unheated and heated ordinary and heavy concrete samples are scanned using thermal neutron emitted from the SINQ facility. The sample was scanned using 200 projections, 0.9° angular step, 255 transmissions, 0.04 mm transmission step (depending on the CCD camera resolution) and of 1 s per projection time.

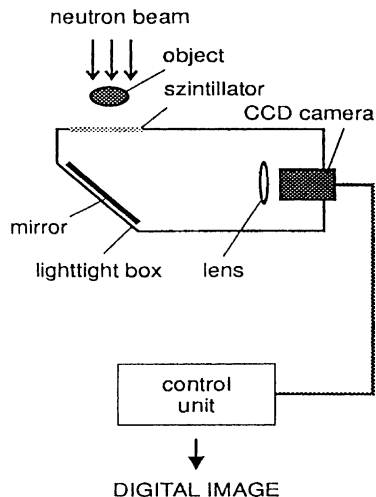


Fig. 3. Basic setup of the type of detector based on the combination of a scintillator screen and a CCD-camera.

4. Results and discussion

The FBP and ART techniques are first tested with simulated object to determine the accuracy, sharpness, resolution... etc. to compare and choose the best of them for application for real measured sample. The simulated object examined consists of a disc of high-density material, with five holes, filled with rods of different densities. Details are given in Table 1. The reconstruction area is $7\text{ cm} \times 7\text{ cm}$.

The FBP technique was first applied without a filtered function, then with the absolute filter function, and finally by the Shepp Logan filter function thus showing the effect of using the different filter function with this technique. Second, the ART technique was applied as an iteration technique and the accuracy was determined to compare between the FBP technique and ART technique.

The reconstructed image of the simulated object using the back projection technique with fast Fourier transformer without filtering is shown in Fig. 4. On the right side of the image the gray scale starts from low densities (dark gray) to high densities (light gray), it must be noted that the density is relative to each other. The displayed image shows that the attenuation coefficient has the highest value at the center of the object and decreases on moving towards the periphery. The image also shows that

Table 1
Geometrical and attenuation parameters of the investigated simulator

Element name	Center coordinates		Diameter (cm)	Attenuation coefficient
	x-Coordinate	y-Coordinate		
Main disc	0.00	0.00	4	0.7
Rode # 1	-1.50	0.00	0.2	-0.6
Rode # 2	-1.00	0.00	0.4	-0.5
Rode # 3	00.00	0.00	0.6	-0.4
Rode # 4	1.00	0.00	0.4	-0.3
Rode # 5	1.50	0.00	0.2	-0.2

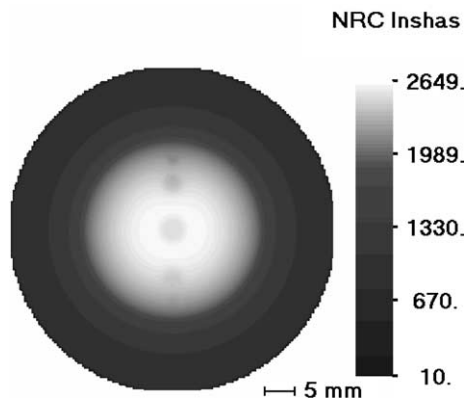


Fig. 4. Image of simulated object with back projection without filtering.

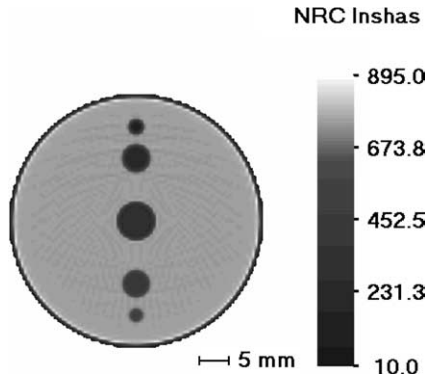


Fig. 5. Image of simulated object reconstructed by FBP with absolute filter function.

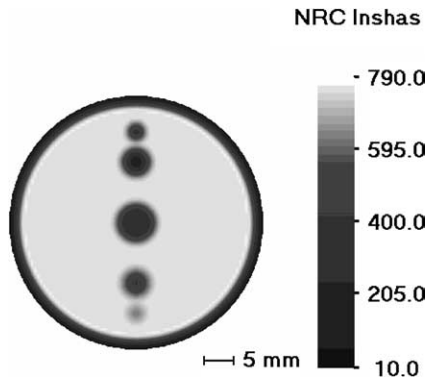


Fig. 6. Image of simulated object reconstructed by FBP with Shepp Logan filter function.

holes number 1, 2, 3, 4 and 5 are blurred, the dimension of all holes is not correct measured and the gray scale is over estimated.

The reconstructed image of the simulated object from the FBP technique with fast Fourier transformer using the absolute filter function is shown in Fig. 5. The displayed image shows that the examined object has a homogeneous density, the rods number 1, 2, 3 and 4 can be seen very clearly, with a uniform and correct dimension. This image also shows that the color of the rods matches well with the rod's density, which was assumed. Moreover, the image indicates that the smallest rod number 5 is shown clearly, i.e., the use of the absolute function give a sharper image with precisely defined edges.

The reconstructed image of the simulated object by the FBP technique with fast Fourier transformer using the Shepp Logan filter function is shown in Fig. 6. The object is of homogeneous density, the rods number 1, 2, 3 and 4 are shown clearly and the dimension is uniform and correct. This image also shows that the color of the rods matches well with the rod's density, which was assumed. However the rod number 5 is blurred. This can be attributed to the smoothing of the Shepp Logan

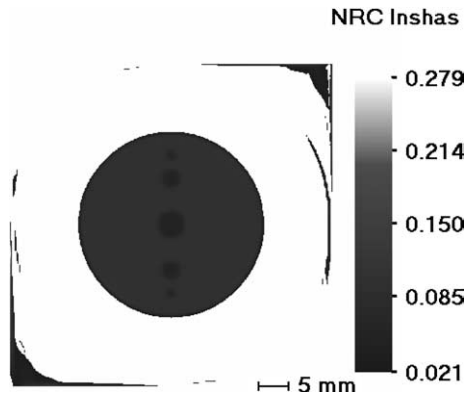


Fig. 7. Image of simulated object reconstructed by ART.

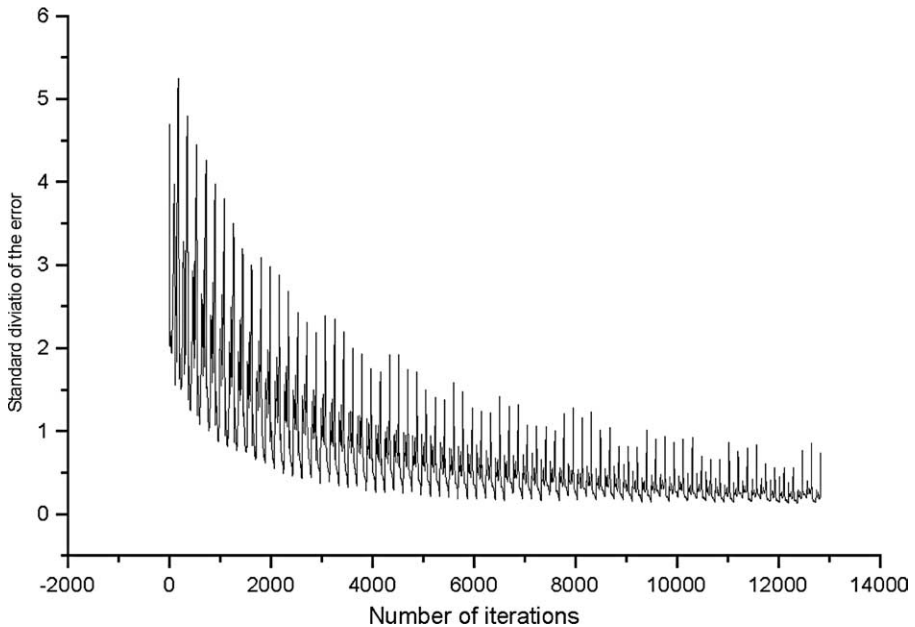


Fig. 8. The accuracy curve during the iteration process.

filter function, which is effective in the high frequency range. This effect of the smoothing can be shown clearly in small sharp edges.

The reconstructed image of the simulated object by the ART technique is shown in Fig. 7. This image indicates that, the examined object is of homogeneous density and all rods have the same attenuation coefficient. The observed attenuation coefficients for the disc and the embedded rods have lower values than the actual ones. This could be attributed to that the used normalization factor is not the proper one. It should be mentioned that the same observed attenuation coefficient for all the rods

indicates that the ART technique has no ability to distinguish between materials of close by densities, but it can differentiate between rods of different diameter where the 2 mm diameter one is shown clearly. The reconstructed image also indicates that, some artifacts are clearly shown at the right top and the left down corners of the reconstructed area. The increasing of the number of iterations may decrease these artifacts. The dimension of the object and the rods is uniform and correct. This can be attributed to the bad density resolution and accepted spatial resolution of the ART technique.

Fig. 8 shows the accuracy of the reconstructed image, during the 12780 iterations. The accuracy is calculated using the standard deviation of $\Delta P(\theta)$.

The profile of the curve is repeated each 180 iterations, and the standard deviation of the error decreases gradually during the iteration. It should be mentioned that the main disadvantage of this technique is the large computational time (355 h on PIII 500 MHz Personal computer) because of its iterative nature.

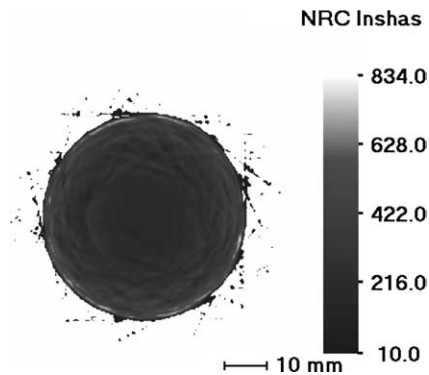


Fig. 9. Thermal neutron image for unheated ordinary concrete sample by using Shepp Logan filter function.

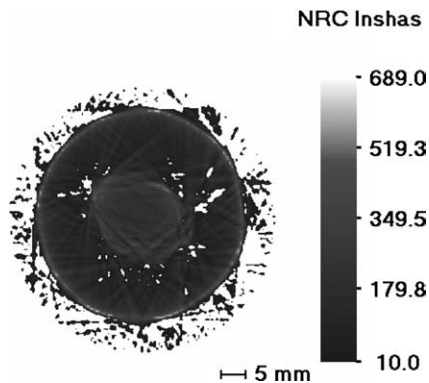


Fig. 10. Thermal neutron image for heated ordinary concrete sample by using Shepp Logan filter function.

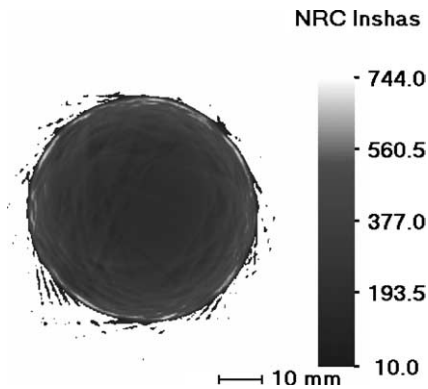


Fig. 11. Thermal neutron image for unheated heavy concrete sample by using Shepp Logan filter function.

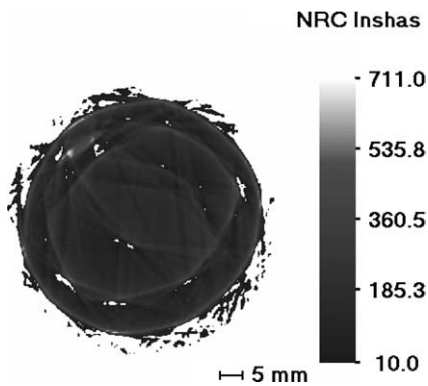


Fig. 12. Thermal neutron image for heated heavy concrete sample by using Shepp Logan filter function.

Figs. 9–12 show the reconstructed images of the unheated and heated concrete samples with Fourier method using Shepp Logan filter function. The displayed images show that the effect of heating tends to decrease the water content of the sample, and therefore the heated samples show lower attenuation coefficient than the unheated one. Creaks of about 0.5 mm can be seen clearly for the heated samples (especially in case of ordinary concrete samples) due to the effect of the heating process. Moreover, images also show that, the examined samples are homogeneous, this means that, the coarse aggregate is of small size and has been mixed well. Moreover, the images are very sharp, that the sample is seen to be consists of lines and the resolution of the images is in the range of 0.45 mm and therefore small details can be seen.

For comparison between absolute and Shepp Logan filter functions, images of the same cross sections will be reconstructed by using absolute filter function. Figs. 13 and 14 show the unheated and heated ordinary concrete images reconstructed by FBP using the absolute filter function. The effect of the heating process can be seen

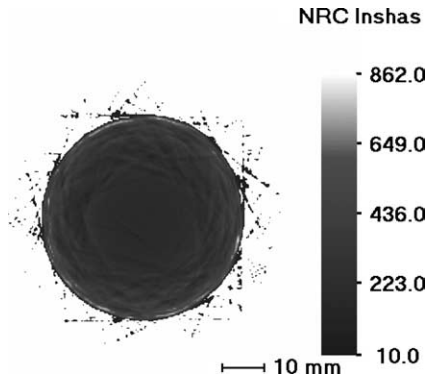


Fig. 13. Thermal neutron image for unheated ordinary concrete sample by using absolute filter function.

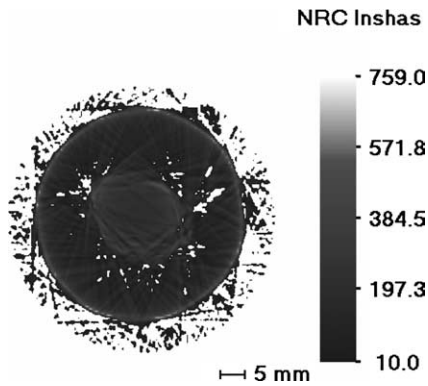


Fig. 14. Thermal neutron image for heated ordinary concrete sample by using absolute filter function.

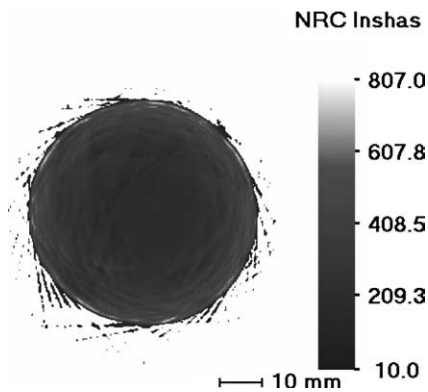


Fig. 15. Thermal neutron image for unheated heavy concrete sample by using absolute filter function.

clearly, where the heated sample shows a lower attenuation coefficient than the unheated one. Cracks of about 5 mm can be seen clearly in the heated sample as a result. Figs. 15 and 16 show the images of the unheated and heated heavy concrete

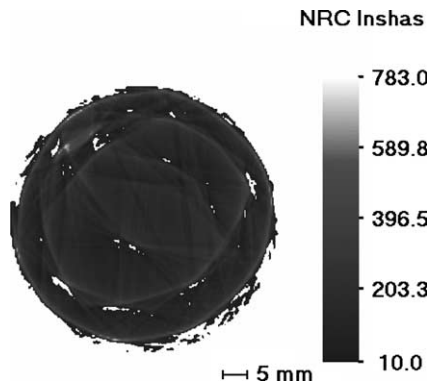


Fig. 16. Thermal neutron image for heated heavy concrete sample by using absolute filter function.

filtered by absolute filter function. Also, the effect of the heat process can be seen clearly where the heated sample has a lower attenuation coefficient than the unheated one. The image in Fig. 16 shows that a small high density spot (light gray spot) at the left top corner can be seen due to the presence of a hematite coarse aggregate. It was seen that the images which have been produced by Shepp Logan filter function has the same resolution as that produced by the absolute filter function. Moreover, the image produced by using Shepp Logan filter function is of higher contrast than that produced using absolute filter function, due to the smoothing of high frequency values in the case of the Shepp Logan filter function.

5. Conclusion

1. The FBP and ART techniques can be successfully used to produce a two-dimensional image from the transmission data.
2. The image produced by the ART technique has poor density resolution, acceptable spatial resolution, large computational time.
3. The images produced by FBP using a Shepp Logan filter function has a higher contrast, and more smoothing than that produced using the absolute filter function.
4. Imaging by thermal neutrons gives more precise information on the water content of the examined samples. This is due to the high scattering cross section of neutrons with hydrogen at thermal neutron energy.
5. The filtered back project technique has the ability to show the homogeneity and cracks within small samples.
6. The displayed images for heated samples indicate that the rate of water loss is more pronounced in case of ordinary concrete especially at the sample periphery.

References

- Ali, A.M., 1998. Materials testing by computerized tomography using neutrons and gamma rays. Master Thesis, Ain Shams University, Cairo, Egypt.

- Avinash, C.K., Malcolm, S., 1999. Principles of Computerized Tomographic Imaging. IEEE Press, New York, USA.
- Lehmann, E.H., Vontobel, P., Wiezel, L., 2001. The investigation of highly activated samples by neutron radiography at the spallation source SINQ. *Nucl. Instrum. Methods Phys. Res. Sect. A* 467, 203–214.
- Pfister, G., Schatz, A., Koch, D., Stier, G., Siegel, C., 1992. Nondestructive testing of materials and components by computerized tomography with fast and thermal reactor neutrons. *Nuclear Science and Engineering* 110, 303–315.
- Pleinert, H., Lehman, E.H., Korner, S., 1997. Design of a new CCD-camera neutron radiography detector. *Nuclear Instruments and Methods in Physics Research A* 399, 382–390.
- Schatz, A., Pfister, G., Koch, D., Stier, G., Siegel, C., 1989. Computer tomography with fast and thermal neutrons. In: *Third World Conference on Neutron Radiography*, May 14–18, 1989, Osaka, Japan.
- Shepp, L.A., Logan, B.F., 1974. The fourier reconstruction of a head section. *IEEE Transactions on Nuclear Science* NS-21 (June).